Computational Analysis of the Binding Poses of Nitazene Derivatives at the μ-Opioid Receptor

Joseph Clayton,[†,‡] Lei Shi,[¶] Michael J. Robertson,[§,#] Georgios Skiniotis,[‖,@] Michael Michaelides,[⊥] Lidiya Stavitskaya,[*,†] and Jana Shen[*,‡]

†*Division of Applied Regulatory Science, Office of Clinical Pharmacology, Office of Translational Sciences, Center for Drug Evaluation and Research, United States Food and Drug Administration, Silver Spring, MD 20993, USA*

‡*Department of Pharmaceutical Sciences, University of Maryland School of Pharmacy, Baltimore, MD 21201, USA*

¶ *Computational Chemistry and Molecular Biophysics Section, Molecular Targets and Medications Discovery Branch, National Institute on Drug Abuse, NIH/DHHS, 333 Cassell Drive, Baltimore, MD 21224, USA*

§*Department of Molecular and Cellular Physiology, Stanford University School of Medicine, Stanford, CA 94305, USA*

‖*Department of Molecular and Cellular Physiology, Department of Structural Biology, Stanford University School of Medicine, Stanford, CA 94305, USA*

⊥ *Biobehavioral Imaging & Molecular Neuropsychopharmacology Section, Neuroimaging Research Branch, National Institute on Drug Abuse, 333 Cassell Drive, Baltimore, MD 21224, USA*

Current address: The Verna and Marrs McLean Department of Biochemistry and Molecular Pharmacology, Baylor College of Medicine, Houston, Texas 77030, USA

@*Current address: Center of Excellence for Structural Cell Biology, Department of Structural Biology, St Jude Children's Research Hospital, Memphis, TN 38120, USA*

E-mail: Lidiya.Stavitskaya@fda.hhs.gov; jana.shen@rx.umaryland.edu

Abstract

Nitazenes, a novel class of synthetic opioids with exceptionally high potency, has recently emerged on illicit markets, resulting in many overdose deaths. Currently, an experimental structure of nitazene bound to the molecular target, the μ-opioid receptor (μOR), is lacking, hindering the understanding of their structure-activity relationships. Here we employed a suite of computational approaches, encompassing consensus docking, metadynamics, and conventional molecular dynamics (cMD) refinement, to determine the putative μOR binding poses of eight nitazenes, including the nitro-containing meto-, eto-, proto-, buto-, and isotonitazene and the nitro-less metodes-, etodes-, and protodesnitazene. Docking generated three possible binding modes, whereby the nitro-substituted or unsubstituted benzimidazole group extends into subpocket 1 (SP1) between transmembrane helix (TM) 2 and 3, subpocket 2 (SP2) between TM2, TM7, and TM1 or subpocket 3 (SP3) between between TM5 and TM6. Metadynamics and cMD simulations suggested that the SP2-binding mode is most stable for etonitazene and analogs as well as etodesnitazene. Based on the comparison to the experimental structures of BU72-, fentanyl- and mitragynine pseudoindoxyl (MP)-bound μOR, we proposed a general model for receptor-opioid recognition, which involves interactions with SP1, SP2 and SP3. The hydrophobic SP1 prefers an aromatic moiety, such as the phenyl ring of BU72 and fentanyl. In contrast, the hydrophilic SP2 and SP3 favor a polar group which can form water-mediated hydrogen bond interactions with the conserved Tyr75$^{1.39}$ and His297$^{6.52}$. Our findings provide molecular insights into the mechanism of receptor-opioid recognition, paving the way for investigations of the structure-activity relationships of nitazenes.

Introduction

The number of deaths due to illicit and prescription opioid overdose has been sharply increasing in the United States, with over 80,000 deaths reported in 2022. Furthermore, over 80% of the deaths are due to synthetic opioids, primarily fentanyl.[1] Fentanyl and other opioids are agonists of the μ-opioid receptor (μOR), a member of the class A family of G-protein coupled receptors (GPCRs). When bound to an agonist, μOR undergoes a conformational change that allows it to associate with G-proteins and β-arrestins; it is hypothesized that the G-protein signalling pathway produces an analgesic effect while the β-arrestin pathway leads to adverse effects including respiratory depression.[2,3] Two antagonists at the μOR, naloxone and nalmefene, have been approved by the FDA as rescue agents to rapidly reverse opioid overdose through competitive binding with agonists such as fentanyl.

In recent years, a new class of synthetic opioids from the 2-benzylbenzimidazole family (also called nitazenes) has emerged on the illicit market (Figure 1). Many of the nitazene derivatives were first invented by a Swiss company in the late 1950s, but were never marketed due to their high potency.[4] Isotonitazene was first found in biological samples in the United States in 2019 and was the subject of a public health warning from the DEA Washington Division in 2022;[5] since then, ten nitazenes have been scheduled by the DEA.[6] Members of this family are known to be up to 20 times more potent than fentanyl.[7–9] A recent study found that overdose patients in the emergency department testing positive for nitazenes required higher dosing of naloxone compared with fentanyl alone and that metonitazene overdose was associated with cardiac arrest and death at a higher rate than other substances.[10]

Figure 1 shows the chemical structure of selected nitazenes. Recent experimental studies showed that nitazenes that contain both a nitro group at R_1 and an alkoxy group at R_2 have a higher potency than other nitazenes.[7,8] For example, etonitazene (R_1=NO_2, R_2=OC_2H_5) has an EC_{50} of 1.71 nM, while the EC_{50} of the nitro-absent counterpart etodesnitazne (R_1=H, R_2=OC_2H_5) is nearly two orders of magnitude higher (164 nM). Nitazenes containing a halogen, clonitazene (R_1=NO_2, R_2=Cl) and flu-

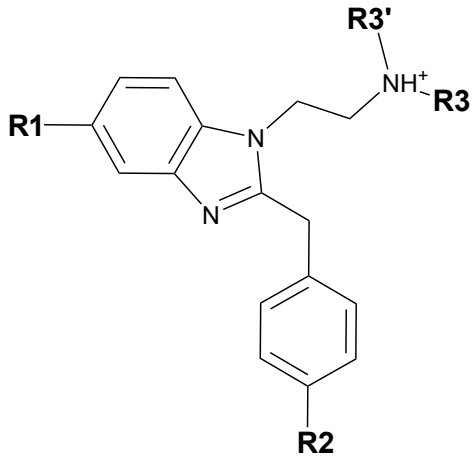

Compound	R1	R2	R3	R3'
Metonitazene	NO_2	OCH_3	C_2H_5	
Etonitazene	NO_2	OC_2H_5	C_2H_5	
Protonitazene	NO_2	OC_3H_7	C_2H_5	
Butonitazene	NO_2	OC_4H_9	C_2H_5	
Isotonitazene	NO_2	$OCH_2(CH_3)_2$	C_2H_5	
Metodesnitazene	H	OCH_3	C_2H_5	
Etodesnitazene	H	OC_2H_5	C_2H_5	
Protodesnitazene	H	OC_3H_7	C_2H_5	
Clonitazene	NO_2	Cl	C_2H_5	
Flunitazene	NO_2	F	C_2H_5	
N-desethyl Isotonitazene	NO_2	$OCH_2(CH_3)_2$	C_2H_5	H
N-pyrrolidino etonitazene	NO_2	OC_2H_5	C_4H_5N	

Figure 1: **Chemical structures of nitazenes.** Nitazenes share a 2-benzylbenzimidazol core with varying substitutions at R_1, R_2 and R_3 positions. R_1 is either occupied by a nitro (NO_2) group or is empty; R_2 is occupied by either a halogen or an -oxy group of varying sizes; R_3 and R_3' are most commonly occupied by ethyl groups, but can also be part of a ring structure such as pyrrolidine. The nitazenes studied in this work are in bold font; all except protodesnitazene are currently Schedule 1 substances.

nitazene (R_1=NO_2, R_2=F), showed an even higher EC_{50} of 338 and 827 nM, respectively.[7]

To date, no experimental structure model of μOR in complex with a nitazene is available, hindering the molecular understanding of the pharmacology and structure-activity relationship of nitazenes. Meto-, eto-, proto-, buto-, and isotonitazenes are Schedule I substances under the U.S. Controlled Substance Act. These nitazenes share nitro group as R_1 and ethyl group as R_3/$R_{3'}$, while the length of the alkoxy group at R_2 varies (Figure 1). In this work, we study these nitazenes and three nitroless analogs (R_1=H), metodes- and etodesnitazene, which are also Schedule I substances, as well as the commercially available protodesnitazene, which has not been scheduled yet (Figure 1). All eight nitazenes were recently found to be at least as potent as fentanyl.[7]

Based on the X-ray co-crystal structures and cryogenic electron microscopy (cryo-EM) models of μOR in complex with agonist ligands, particularly BU72, fentanyl, and mitragynine pseudoindoxyl (MP), we analyzed the possible binding poses of the eight nitazenes (Figure 1). We used consensus docking followed by pose re-ranking with the binding pose metadynamics (BPMD) protocol,[11,12] as well as refinement with the conventional molecular dynamics (cMD). Two possible binding modes for the nitro-containing nitazenes were found, which differ in positioning of the nitro group, akin to the phenylethyl group of fentanyl in subpocket 1 (SP1) or the indole group of MP in subpocket 2 (SP2). For etonitazene, the SP2-binding mode was estimated to be favored by 2–4 kcal/mol based on the well-tempered metadynamics (WT-metadynamics) simulations[13] of the refined SP1 and SP2-binding poses. For the nitro-less nitazenes, the SP1-binding mode was ruled out based on the cMD simulations of etodesnitazene bound μOR. Finally, the analysis of putative binding modes of nitazenes and comparison to the experimental structures of other μOR:agonist complexes led to a proposed model for the molecular recognition of opioids by μOR.

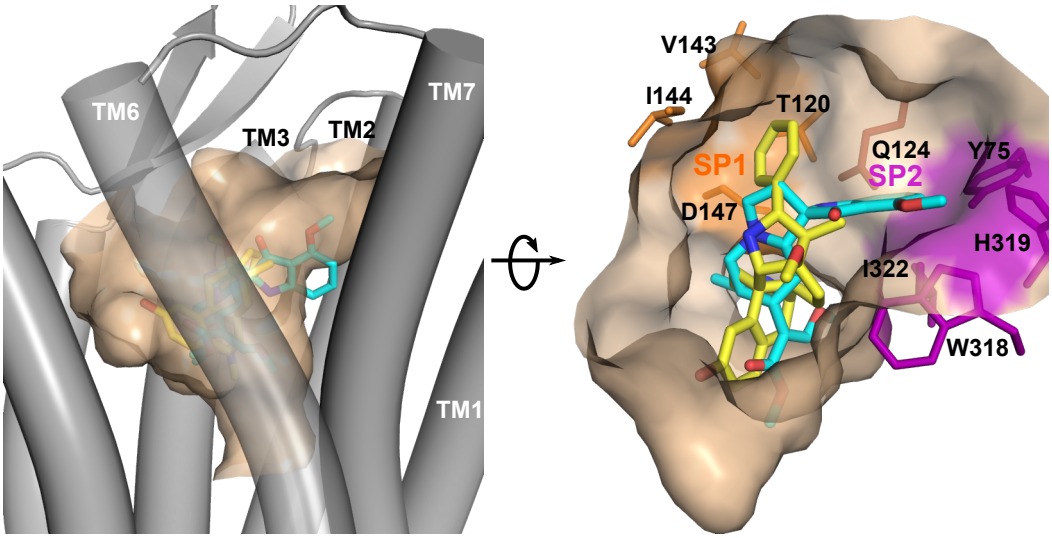

Figure 2: **Visualization of the binding pocket of μOR in complex with BU72 (yellow; PDB: 5C1M[14]) or MP (cyan; PDB: 7T2G[15]).** For comparison, the BU72 and MP structures are superimposed; but the MP-bound μOR structure is hidden. A main difference is that BU72 reaches into subpocket 1 (SP1, orange) between TM2 and TM3, while MP extends into subpocket 2 (SP2, purple) between TM2 and TM7. SP1 and SP2 are separated by Gln124.

Results and Discussion

Analysis of the experimental structure models of μOR-ligand complexes

To understand the ligand binding site, we examined the published structure models of all 14 agonist-bound μOR complexes, including one X-ray structure and 14 cryo-EM structure models (Supplemental Table S1). These structures show that the ligand occupies the same central cavity of μOR, and a part of the ligand, e.g., the phenyl group of BU72 or the phenethyl group of fentanyl, reaches into the space between TM2 and TM3, referred to as subpocket 1 (SP1) in Ref,[15] comprising of Thr120 (Thr$^{2.57}$ in Ballesteros-Weinstein numbering[16]), Val143$^{3.28}$, Ile144$^{3.29}$, and Asp147$^{3.32}$ (Figure 2). The only exception is shown by the cryo-EM model of the mitragynine pseudoindoxyl (MP)-bound μOR (PDB: 7T2G),[15] in which the methoxyphenyl group extends into the space between TM2 and TM7 (subpocket 2 or SP2,[15] Figure 2 and S1) comprised of Tyr75$^{1.39}$, Trp318$^{7.34}$, His319$^{7.35}$, and Ile322$^{7.38}$. Considering that the structure of μOR in complex with BU72 (PDB: 5C1M)[14,17] has the highest resolution (2.1 Å) and the BU72 interaction with SP1 is shared with 13 other agonists, we selected it as the template for the docking campaign of nitazenes first.

Validation of the docking and re-ranking protocol using fentanyl

Three binding modes were generated by the docking software. Three docking software, AutoDock Vina,[19] Glide[20] (part of the Schrödinger software suite), and MOE[21] were utilized to examine whether the binding pose of fentanyl in the recent cryo-EM model (PDB: 8EF5)[18] can be recapitulated using the BU72-bound μOR structure (PDB: 5C1M)[14,17] as a template. Binding poses were generated using the three software. For each software, the top three ranked poses were similar in their affinity score (with difference in the second digit or within 1-5% difference) and yet the ligand conformation was significantly different in some cases (Figure 3). Specifically, the generated poses can be grouped into three categories based on the placement of the propanamide, phenyl, and phenylethyl motifs. The pose is referred to as Match if the positions of all three motifs are similar as in the cryo-EM structure

Software	Affinity/ Score	Category
Autodock (kcal/mol)	-9.82	Match
	-9.70	Flipped
	-9.67	Flipped
Glide (Score)	-5.87	Akin
	-5.84	Match
	-5.36	Match
MOE (kcal/mol)	-7.99	Flipped
	-7.82	Flipped
	-7.67	Flipped

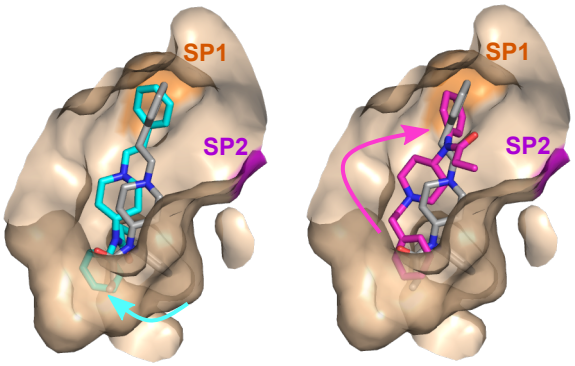

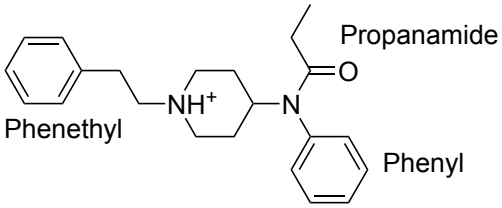

Figure 3: **Molecular docking generates three unique poses of fentanyl in μOR. Left:** The top three ranked binding poses and their scores given by three docking software. The best score for each category is given in Table S2. Each pose is labeled as Match, Akin, or Flipped based on the fentanyl position relative to the cryo-EM structure model of the fentanyl-mOR complex (PDB: 8EF5).[18] **Right:** Overlay of the cryo-EM (wheat) and the two docked poses that differ: in Akin (cyan), the phenylethyl group is placed in SP1 between TM2 and TM3, but the propanamide and phenyl groups are swapped in positions; in Flipped (magenta), the phenylethyl and phenyl groups are swapped in positions. For reference the two-dimensional structure of fentanyl is given below.

model (PDB 8EF5, Figure 3). The next category is largely similar, except that the locations of the propanamide and phenyl groups are swapped; since the phenylethyl is still placed in a hydrophobic region towards the extracellular entrance, this category is dubbed "Akin" (Figure 3). Finally, a third category swaps the positions of the phenylethyl and phenyl groups, resulting in a 180° flip, dubbed "Flipped" (Figure 3). Note, this pose was reported in several previous computational work[22–24] and was shown to have similar stability in metadynamics simulations.[25] It is worth noting that all three software generated at least one Match pose; however, the scoring function utilized could not differentiate the Match pose from others (Table S2).

The Match pose of fentanyl is most stable in BPMD. It is common knowledge that the true binding pose is often among the poses generated by a docking program, it is often not the most favorable one based on the docking score.[11] Since the docking scores for the poses are highly similar, we tested an empirical protocol called binding pose metadynamics (BPMD)[11,12] to re-rank them by assessing the relative stabilities of the poses in the receptor using metadynamics simulations. Briefly, each pose was used to initiate ten runs of 10-ns metadynamics simulations, whereby the ligand heavy-atom root-mean-square deviation (RMSD) with respect to the initial coordinates as the collective variable (details see Methods). Each pose was analyzed by measuring the evolution of two quantities: the RMSD of the ligand with respect to the predicted pose, and the distance between the piperidine nitrogen of fentanyl and the nearest carboxylate oxygen of Asp147$^{3.32}$. The RMSD reveals the amount that the biasing potential is able to push the ligand away from its initial pose, while the distance indicates if the conserved salt-bridge interaction[14] remains intact. The most stable pose should have the lowest average RMSD (over the ten trajectories) and consistently maintain the salt bridge between piperidine and Asp147$^{3.32}$. Representative poses were tested by first clustering generated poses (sep-

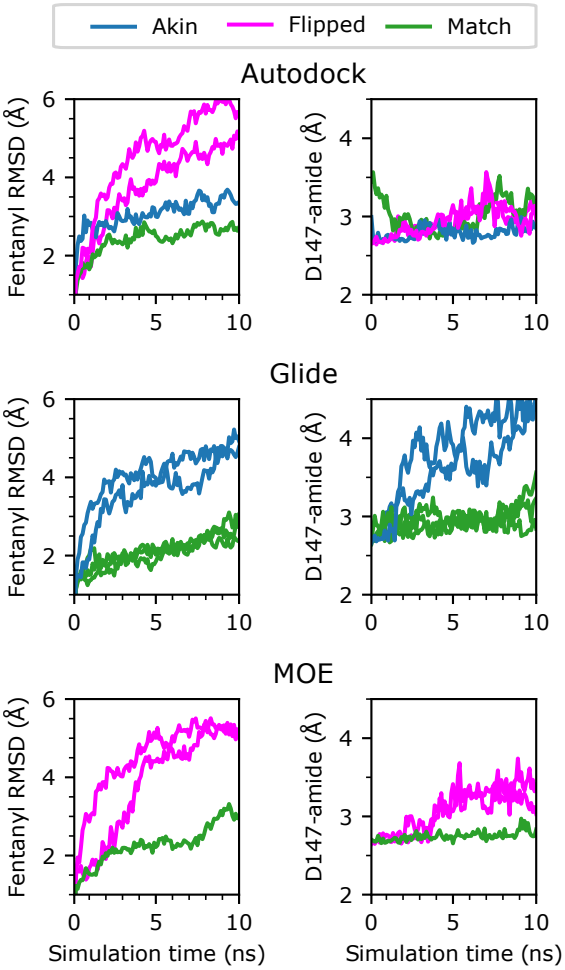

Figure 4: **Binding pose metadynamics protocol showed that the Match pose is most stable in μOR.** Two quantities used to evaluate the three categories of poses, averaged per frame over ten 10-ns trajectories. **Left panel:** the average minimum distance between the piperidine amine nitrogen of fentanyl and the carboxylate oxygens of Asp147$^{3.32}$ as a function of simulation time. **Right panel:** the average heavy atom RMSD of fentanyl with respect to the docked pose as a function of simulation time.

arated by software), then the centroid of each cluster was tested. Figure 4 shows the evolution of each quantity for these tested poses, averaged over the ten simulations, and colored by the category the tested pose belonged to. Encouragingly, for the poses generated by all three docking tools, the Match pose consistently had the lowest average RMSD and maintained an average salt bridge distance of ∼3 Å. In contrast, the Flipped or Akin poses consistently had higher average RMSD with some disruption in the conserved salt bridge. Moreover, poses that flip the ligand and place the phenylethyl closer to the center of the receptor pocket had a final average RMSD of 2-3 times larger than the most stable poses. These results suggest that BPMD is capable of differentiating between similarly scored poses, and in this case, finding the experimentally determined pose.

Determination of the putative binding poses of nitazenes

Docking based on the μOR:BU72 co-crystal structure places the nitro group in SP1 or SP3. Having validated the docking and ranking protocol, we proceeded with predicting the nitazene binding poses. Eight nitazenes were studied, five of which contain a nitro group at R1 while the remaining three do not (Figure 1). With the constraint of triethylamine and Asp147$^{3.32}$ salt bridge formation, the docked poses from the three software were categorized based on whether the nitro group or the benzene of the benzimidazole motif for the nitro-less nitazenes was placed in SP1 between TM2 and TM3 or another subpocket between TM5 and TM6, which will be referred to as SP3 hereafter (Figure 5 and Table S3). In the SP1-binding mode, the alkoxy group of the nitazene is placed into SP3, whereas in the SP3-binding mode, it is placed in SP1. In other words, the positions of alkoxy and nitro (or benzene for nitro-less nitazenes) groups are swapped. It is noteworthy that some software only generated the SP1-binding mode for some nitro-containing nitazenes, e.g., Glide generated only the SP1-binding mode for meto-, eto-, buto-, and isotonitazenes (Figure 5a). Curiously, Autodock predicted a third category of poses, dubbed SP2', where the nitro group was placed on top of Gln124$^{2.60}$ and pointed towards TM1, the *N*-diethyl occupied SP1, and the oxyl tail oriented downward towards the center of the receptor (Figure S4). Thus, for simplicity this pose is not visualized in Figure 5.

The SP1-binding mode is more stable than the SP3 binding mode for the nitro-containing nitazenes. To assess which pose, i.e., SP1 or SP3, is more stable, we performed BPMD on the poses generated by the three software for all eight nitazenes. For the nitro-containing nitazenes (meto-, eto-, proto- and butonitazene), the SP1 poses are consistently more stable than the SP3 poses (Figure 5a). For the nitro-less analogs, metodes-, etodes-, and protodesnitazene, however, there is no consistent trend when considering any one compound across the three software or any one software across the three compounds (Figure 5b). For example, considering metodesnitazene, the SP3 pose is favored by two software Glide and Autodock, whereas the SP1 pose is favored by MOE. However, for etodesnitazene, the SP1 pose is favored by two software Glide and Autodock, whereas the SP3 pose is favored by MOE. When considering a single software, e.g., Glide, it only produced SP3 poses for meto- and protodesnitazenes; however, it favored the SP1 pose for etodesnitazene.

Docking based on the μOR:MP cryo-EM model places the nitro group in SP2. As our analysis of the experimental structure models of agonist-bound μOR showed that the SP2 between TM2 and TM7 can also be occupied as in the cryo-EM model of the μOR:MP complex (PDB: 7T2G),[15] we used the latter model to dock the eight nitazenes. Note, the SP1 occupied by BU72, fentanyl, and 11 other ligands and the SP2 occupied by MP are separated by Gln124$^{2.60}$; which can block one of the subpockets due to the movement of the methylamide group (related to a χ_2 angle change). In the BU72-, fentanyl- and 11 other agonist-bound μOR structures (PDB 5C1M and 8EF5, Table S1), the methylamide group of Gln124$^{2.60}$

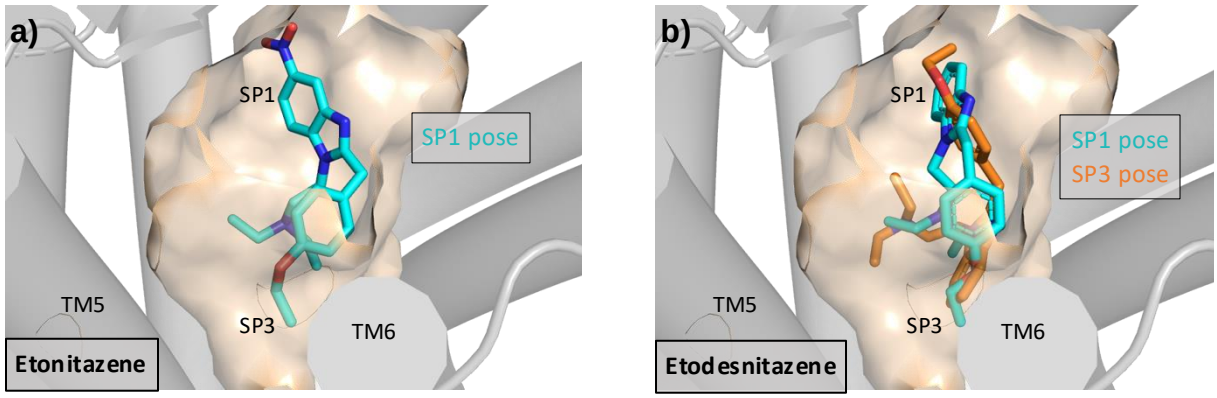

	Meto-	Eto-	Proto-	Buto-	Isoto-
R2:	OCH_3	OC_2H_5	OC_3H_7	OC_4H_9	$OCH_3(CH_3)_2$
Glide	SP1*	SP1*	SP1	SP1*	SP1*
MOE	SP1*	SP1	SP1	SP1	SP1
Autodock	SP1	SP1	SP1	SP1	SP1

	Metodes-	Etodes-	Protodes-
R2:	OCH_3	OC_2H_5	OC_3H_7
Glide	SP3*	unclear	SP3*
MOE	unclear	unclear	unclear
Autodock	SP1*	SP1*	unclear

Figure 5: **Predicted stable poses of eight nitazenes based on the BU72-μOR co-crystal structure and BPMD.** The pose category that was most stable in the BPMD trajectories is given for the nitro-containing (a) and nitro-less nitazenes (b). An asterisk indicates that the software only predicted poses in that particular category.

points down, opening the entrance to SP1 but blocking that to SP2. In contrast, the μOR-MP complex structure 7T2G shows that the methylamide group points up and towards TM3, blocking the entrance to SP1 but opening that to SP2.

Docking of the eight nitazenes based on the cryo-EM model of the μOR-MP complex (PDB 7T2G) resulted again in two distinct binding modes – each determined by whether the nitro group (or the benzene ring) is placed in the opened SP2 or the lower SP3 (Figure 6left and Table S4). In the former pose, the alkoxy group extends towards SP3, whereas in the latter pose it points towards SP1. This result indicates that the SP1- and SP2-bound nitazene poses are mutually exclusive, as neither structure template produced both poses. This also means that BPMD cannot be used to evaluate the relative stability between the SP1- and SP2-binding modes.

For the nitro-containing nitazenes, the SP3-binding mode was only produced by MOE (Table S4) and its docking score relative to the SP1-binding mode is inconsistent among meto-, eto-, proto-, buto-, and isotonitazenes. Thus, the SP3 binding pose will not be further discussed for the nitro-containing nitazenes. For the nitro-less nitazenes, the docking scores of the SP2 and SP3 binding poses for the three programs suggest that SP2-binding mode is more stable (Table S4).

The SP2-binding mode is more stable than the SP1-binding mode for etonitazene. To determine which of two poses (SP1 or SP2) is more favorable, we used etonitazene as an example and estimated the free energy difference between the two poses using WT-metadynamics simulations,[13] in which a time-dependent biasing potential was deposited on two collective variables (CVs) representing the distance of the nitro group to SP1 or SP2. The CV1 or CV2 is defined as the distance from the nitro nitrogen to the center of mass (COM) of TM2/TM3 or TM2/TM7, respectively (see Methods). A CV1 of 4 Å is representative of the SP1-binding mode, whereas a CV2 of 4 Å

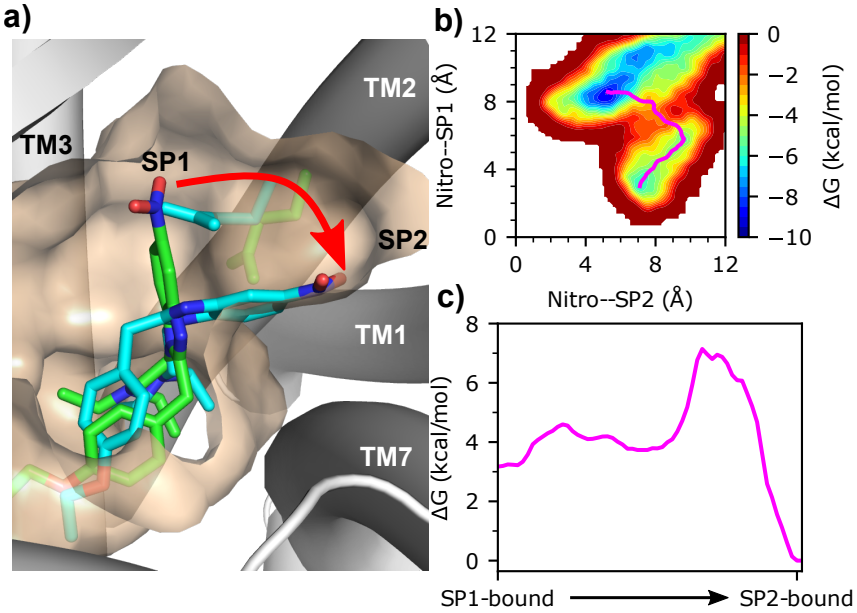

Figure 6: **The SP2-binding mode is more favorable than the SP1-binding mode for etonitazene. a)** Visualization of the initial SP1-binding mode (green) and the target SP2-binding mode (cyan) in the metadynamics simulations. **b)** Estimated free energy landscape as a function of the two collective variables (CVs) from a representative metadynamics trajectory. The resulting minimum free energy path from the nudged-elastic band (NEB) calculation is shown in magenta. **c)** Estimated free energy change going from the SP1- to the SP2-binding mode along the minimum free energy path shown in b).

is representative of the SP2-binding pose.

Five independent 200 ns metadynamics simulations were performed starting from the refined SP1-binding mode of etonitazene through 100 ns cMD, from which the estimated free energy surfaces as a function of the two CVs were obtained (Figure 6 right). While etonitazene in all five trajectories transitioned out of SP1 within 200 ns, the SP2-binding mode were sampled in three trajectories and was more stable than the SP1-binding mode (Figure S5). In each trajectory, once the nitro group moved away from SP1, the χ_2 of Gln124$^{2.60}$ changed from *trans* to *gauch+* (Figure S6), suggesting that an induced fit mechanism may be responsible. That is, the precise binding mode, SP1 vs. SP2, is dependent on the ligand structure. To understand the transition pathway and estimate the free energy difference between the two binding modes, we utilized the nudged elastic band (NEB) method[26] to find the minimum energy path on the free energy landscape estimated by the metadynamics simulation (Figure 6b and c). From the three metadynamics trajectories that sampled the SP2 pose, all show that SP2 pose is more stable than the SP1 pose by 2-4 kcal/mol (Figure 6 and Figure S5).

The SP2-binding mode is more stable than the SP1- and SP3-binding modes for etodesnitazene. We now turn to the nitroless nitazenes. Unlike the nitro-containing nitazenes, no consensus binding mode was found based on the BU72-μOR co-crystal structure using the three docking programs, e.g., Glide only generated the SP3 mode for metodes- and protodesnitazene whereas Autodock only generated the SP1-binding mode for metodes- and etodesnitazene (Figure 2 and Table S3). The BPMD simulations of the SP1 and SP3 binding poses for cases where both poses were predicted by the docking software were also inconclusive (Figure 2 and Figure S3). However, when comparing the SP2 and SP3 poses obtained from the MP-μOR structure based docking, the SP2 pose appears to be preferred (Table S4).

To test which binding pose is the most fa-

vorable for the nitro-less nitazenes, we used etodesnitazene as a model and conducted cMD simulations starting from the docked SP1, SP2, or SP3 pose. Three independent simulations of 200 ns were conducted for each pose, with the first 100 ns used for pose refinement and the last 100 ns used for analysis. To assess the stability of each pose, we examined the distance between the carbon that connects with the nitro nitrogen and the center of mass of the subpocket (see Methods for pocket definitions). In simulations initialized from the SP1-binding pose, benzimidazole consistently moved further away from SP1 (Figure 7 top and Figure S7). Curiously, the χ_2 angle of Gln124$^{2.60}$ changed from *trans* to primarily *gauche+* after 20 ns in all three simulations (Figure S7), similar to that of etonitazene as it transitions from the SP1 to the SP2-binding mode (Figure 6 and Figure S6). This change in the χ_2 angle allows the carboxamide group to move into SP1, pusing the benzimidazole group out of SP1. Thus, it appears that in the absence of a nitro group the benzimidazole is incapable of keeping Gln124$^{2.60}$ out of SP1. Similarly, the benzimidazole also moved away from SP3 in the simulations initiated from the SP3-binding pose, although to a lesser degree (Figure 7 bottom and Figure S7). In contrast, in two of the three trajectories, the SP2-binding pose is stable, and the most probable distance matches that of the initial pose (Figure 7 middle and Figure S7). Additionally, we examined the heavy-atom RMSD of etodesnitazene with respect to the initial pose. Starting in the SP2-binding pose, the RMSD remained below 2 Å in the final 100 ns of two trajectories; in contrast simulations starting from the SP1 and SP3 poses ended with RMSD values above 3 Å (Figure S7). All the above data suggest that the SP2-binding mode is the most stable one.

A general model for μOR-opioid recognition

After establishing that the SP2-binding mode is most stable for etonitazene and etodesnitazene, we hypothesized the SP2 mode is also most stable for other nitazenes. To create a general model for μOR-opioid recognition, we refined

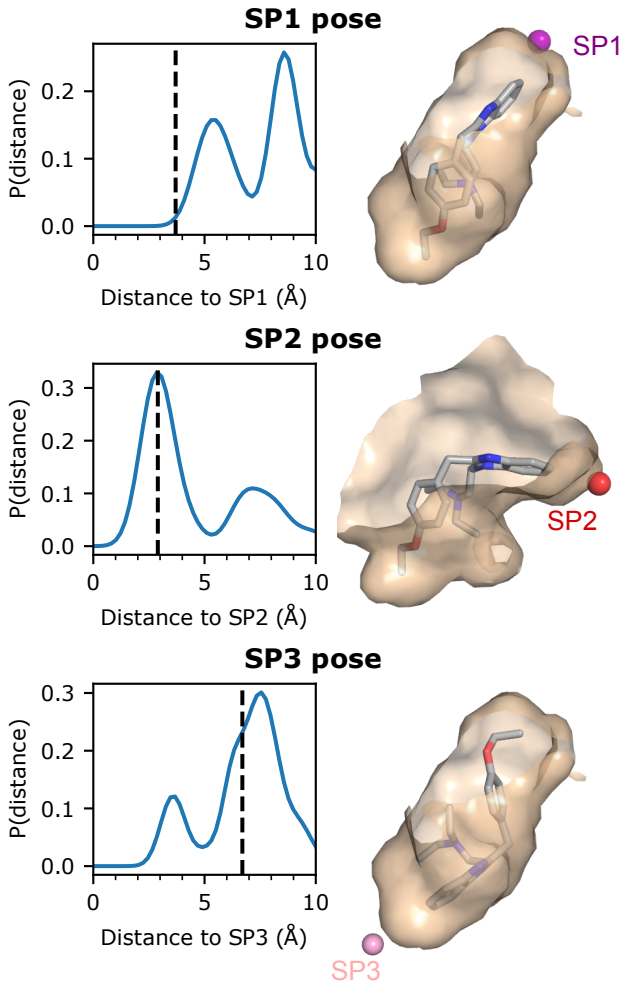

Figure 7: **The SP2-binding is more stable than the SP1- and SP3-binding modes for etodesnitazene. Left panel.** Probability distribution of the distance between the benzimidazole of etodesnitazene and the subpocket SP1 (top), SP2 (middle), and SP3 (bottom). The dashed line indicates the distance measured from the docked pose. **Right panel.** Visualization of the initial SP1-binding (top), SP2-binding (middle), and SP3-binding (bottom) poses. The reference point for each pocket is shown as purple, red, and pink spheres for SP1, SP2, and SP3 respectively. These points are defined as the center of mass of atoms on TM2 and TM3 (SP1), TM2 and TM7 (SP2), and TM5 and TM6 (SP3).

the docked models using 100 ns cMD simulations starting from the SP2-binding modes of meto-, eto-, proto-, buto-, and isotonitazenes. These compounds were tested as they are the most potent nitazenes.[7,8] Note, the simulation of etonitazene was continued to 300 ns and no visible position or conformational change of the ligand was observed (Figure S8). We then compared the binding poses of these nitazenes with those of fentanyl and MP from the cryo-EM structures in an attempt to understand the general trend in the molecular interactions between μOR and opioids with different chemical scaffolds.

Figure 8a visualizes how fentanyl, MP, and etonitazene bind within the receptor pocket. All three utilize a tertiary amine as part of their scaffolds to form a salt bridge with Asp147$^{3.32}$, which anchors the molecule in the central cavity of the receptor. In the cryo-EM model of μOR:fentanyl complex (PDB 8EF5),[18] fentanyl is oriented vertically, whereby the phenethyl group occupies the hydrophobic SP1 and forms hydrophobic contacts with Val143$^{3.28}$ and Ile144$^{3.29}$ between TM2 and TM3. In contrast, the hydroxyl-substituted indole of MP and nitro-substituted benzimidazole of nitazenes occupy the more hydrophilic SP2, interacting with Tyr75$^{1.39}$, His319$^{7.35}$, and Ile322$^{7.38}$. Note, Gln124$^{2.60}$ separates SP1 and SP2; for fentanyl it rests on the bottom of SP2 while for MP and nitazenes it orients towards V143$^{3.28}$. Each tested nitro-containing nitazene utilize the nitro group to form a water-mediated hydrogen bond with Tyr75$^{1.39}$, whereby either oxygen of the nitro group acts as a hydrogen bond acceptor for a water molecule while the hydroxyl oxygen of Tyr75$^{1.39}$ acts as a donor.

It is worthwhile noting that based on the relative orientation and distance, the methoxy oxygen of MP and the hydroxyl oxygen of Tyr75$^{1.39}$ in the cryo-EM model (PDB 7T2G[15]) may form a water-mediated hydrogen bond, similar to the nitro group of the tested nitazenes (Figure 8b). However, when the nitro group is absent, e.g. for etodesnitazene, such a water-mediated interaction does not occur. This may explain the significantly lower binding affinity and potency of the des analog compared to the parent nitro-containing nitazene.[8]

Finally, all of these opioids make hydrophobic interactions with the residues flanking SP3, including Val236$^{5.43}$, His297 $^{6.52}$, and Val300$^{6.55}$. Curiously, only eto-, etodes-, and protonitazenes are capable of interacting with Phe237$^{5.44}$ which lies deep in SP3 towards the lipid bilayer. In the case of butonitazene, the butoxy tail escaped the SP3 pocket in the simulations and extended upwards along TM5, interacting with the sides of SP3. Note, the presence of His297 $^{6.52}$ allows stabilization of polar groups via water-mediated interactions, e.g., two water bridges the interaction between Nδ of His297$^{6.52}$ and the hydroxyl oxygen of BU72 in the X-ray structure (PDB 5C1M).[14] Additionally, metadynamics simulations suggested that His297$^{6.52}$ may directly interact with fentanyl and analogs in the ligand-μOR unbinding process.[25,27] Although water is not resolved in the cryo-EM structure of MP-bound μOR (PDB 7T2G),[15] the distance between the methoxy oxygen and either of the His297$^{6.52}$ imidazole nitrogens is under 5 Å, suggesting that water-bridged interactions are possible too. Similarly, in the SP2-binding mode of nitazenes, water-bridged interactions between the alkoxy group and His297$^{6.52}$ are conceivable, though not observed in our simulations.

Conclusions

In this work, we sought to obtain models of the nitazene-μORinteractions using docking and MD tools. We first tested a protocol comprised of consensus docking based on the μOR:BU72 X-ray structure (PDB 5C1M)[14,17] followed by BPMD. This protocol was able to recapitulate fentanyl's binding pose in the cryo-EM model (PDB 8EF5),[18] in which phenethyl occupies a subpocket SP1. We next applied the protocol to determine the binding poses of five nitro-containing and three nitro-less nitazenes based on the aforementioned μOR:BU72 X-ray structure (PDB 5C1M)[14,17] as well as the μOR:MP cryo-EM model (PDB 7T2G),[15] in which MP occupies an adjacent subpocket SP2 while SP1 (occupied by fentanyl in PDB 8EF5)

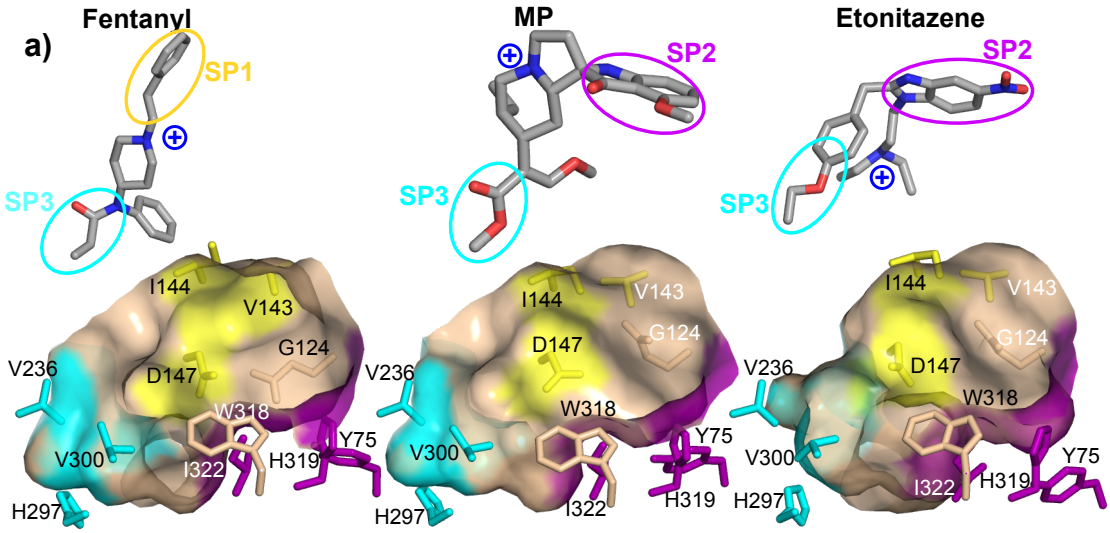

b)

	SP1				SP2				SP3			
	V143 3.28	I144 3.29	D147 3.32	Q124 2.60	Y75 1.39	H319 7.35	I322 7.38	W318 7.34	V236 5.43	F237 5.44	H297 6.52	V300 6.55
Fen.												
MP												
Meto-												
Eto-												
Proto-												
Isoto-												
Buto-												
Etodes-												

Salt bridge
Water mediated
Nonpolar

Figure 8: **Comparison of the μOR binding modes of select nitazenes with fentanyl and MP. a)** Three dimensional structures of fentanyl (PDB 8EF5[18]), MP (PDB 7T2G[15]), and etonitazene (top) and their associated binding pockets (bottom). Subpockets SP1, SP2, and SP3 are colored yellow, purple, and cyan, respectively. **b)** Contact analysis of fentanyl, MP, five nitro-containing nitazenes, and one nitro-less nitazene. Hydrophobic (grey) and salt bridge interactions (dark blue) are defined using a heavy atom distance cutoff of 4.5 Å. For the nitazenes, these interactions with at least 50% occupancy in the final 50 ns are considered. Water-mediated hydrogen bonds (light blue) are included if they have at least 20% occupancy in the final 50 ns. Two possible water-mediated hydrogen bond interactions involving MP are indicated by blue stripes. For simplicity, the following residues are not shown: N127$^{2.63}$ and W133$^{23.50}$ (SP1), S125$^{2.61}$ and Y128$^{2.64}$ (SP2), K233$^{5.40}$ and I296$^{6.51}$ (SP3).

is blocked by Gln124$^{2.60}$. Docking based on the μOR:BU72 template generated the SP1 and SP3 binding modes, while the SP2-binding mode was generated by the μOR:mP template.

Subsequent BPMD and metadynamics simulations suggest that the SP2-binding mode is most stable for etonitazene and likely also meto-, proto-, isoto-, and butonitazenes. The MD data suggest that the SP2-binding mode is stabilized by the water-mediated hydrogen bond interactions between the R1 nitro group of the nitazenes and Tyr75$^{1.39}$ of the receptor. As to the nitro-less nitazenes, the SP2-binding mode may be the most stable one for etodesnitazene. The cMD simulations showed that, unlike fentanyl's phenethyl group that occupies SP1, the unsubstituted benzimidazole group is unable to displace Gln124$^{2.60}$ from SP1, making the SP1-binding mode unfavorable (see below).

Our analysis of the putative nitazene binding modes and comparison to the BU72, fentanyl, and MP binding modes led us to propose a general model for μOR recognition of opioids. In this model, the ligand is anchored to TM3 through a salt bridge between the charged tertiary amine located near the center of the structure and Asp147$^{3.32}$, while the the substituents R1, R2, and R3 (Figure 1) are recognized by the subpockets: SP1 (between TM2 and TM3), SP2 (between TM2 and TM7), and SP3 (between TM5 and TM6). Separated by Gln124$^{2.60}$, the hydrophobic SP1 and hydrophilic SP2 are alternately accessible; the former prefers an aromatic moiety, e.g., the phenyl ring in BU72 or fentanyl, and the latter favors a polar group, e.g., the methoxy group in MP or the nitro group of nitazenes, which can form a water-mediated hydrogen bond interaction with Tyr75$^{1.39}$. The SP3 is largely hydrophobic; however, it contains His297$^{6.52}$, which may stabilize a polar group via water-mediated hydrogen bond interactions, e.g., with the methoxy tail of MP or the alkoxy tail of the nitazenes.

Current work has several caveats worth mentioning. For the nitro-less nitazenes, while the SP1-binding mode is ruled out and the SP2-binding mode appears most stable for etodesnitazene, the stability of the SP3 binding mode, especially for other nitro-less nitazenes, warrants further investigation. Another caveat is the relatively short (100-ns) simulation length for pose refinement, although extending the simulation to 300 ns did not result in a significant shift in the position of etonitazene. We should also note that the simulations were conducted without the G-protein complex, which stabilizes the activated state;[14] simulations on a longer timescale might risk conformational changes away from the activate state. Despite the limitations, our study provides valuable insights into the molecular recognition of nitazenes and other opioids by the μOR, laying the foundation for detailed investigations into the structure-activity relationships.

Methods

Molecular docking of fentanyl

The molecular docking of fentanyl was conducted based on the co-crystal structure of μOR:BU72 complex (PDB: 5C1M)[14] after reversing the modification to Cys57. The nanobody mimicking the G-protein complex was removed, as well as any lipids. The three-dimensional structure of fentanyl was downloaded from PubChem; the piperidine nitrogen of fentanyl was protonated, using the tools in Maestro (before using Glide) or MOE or PyMol v2.5 (before using Autodock-Vina).

Docking with Glide. μOR was prepared using the protein preparation wizard[28] in Maestro and fentanyl was prepared using LigPrep. A docking grid centered around BU72 was created, with a distance constraint between the piperidine nitrogen of fentanyl and Asp147$^{3.32}$. This grid consisted of two parts: a 10x10x10 Å inner box that constrained the center of the docked ligand, and an outer box that was used to compute the grid potentials. The size of the outer box was determined automatically using the size of BU72. A maximum of 10 poses was generated using Glide[20] using standard precision (SP).

Docking with MOE. μOR was first prepared within MOE2022.02,[21] then docking was initiated after identifying the binding pocket based on the position of BU72 and setting a pharmacophore filter to ensure a hydrogen bond with Asp147. 50 poses were generated using London dG scoring function and the triangle matcher method for placement, with 25 being refined using GBVI/WSA dG function.

Docking with AutoDock Vina. Both μOR and fentanyl were prepared using AutodockTools.[29] All nonpolar hydrogens were removed. Docking was confined to a 20x20x25 Å box centered on BU72; exhaustiveness was set to 250, maximum number of poses to 100, and the affinity range to 10 kcal/mol. Generated poses were filtered to ensure a salt bridge with Asp147, defined by a distance cutoff of 4.0 Å between the piperidine amine nitrogen of fentanyl and the nearest carboxylate oxygen of Asp147 and ensuring that the amine hydrogen is oriented towards the carboxylate. Version 1.2.3 of AutoDock Vina[19,30] was used.

Molecular docking of nitazenes

Molecular docking of nitazenes was performed using either the μOR:BU72 complex (PDB: 5C1M[31]) or the μOR:MP complex (PDB: 7T2G[15]). The former was prepared as described for fentanyl, while the latter was prepared in a similar manner (i.e. removal of the G-protein complex and resolved ligands). The three-dimensional structure of each tested nitazene was taken from PubChem; the structure of protodesnitazene was generated by modifying the three-dimensional structure of protonitazene as there was no existing entry for protodesnitazene. The docking procedure and parameters for fentanyl outlined above were used for nitazenes.

Pose evaluation

Selecting poses. For most compounds Glide generated less than the maximum ten poses. The five best scoring poses (or all poses if less than five were generated by Glide) were used to initiate BPMD simulations. In contrast, MOE and Autodock generated a larger amount of poses. To narrow down the poses for evaluation, each pose set (excluding poses with an unfavorable, positive score) was clustered using hierarchical clustering (as implemented in CPPTRAJ[32]) based on the pairwise root-mean-square deviation (RMSD) of the ligand. Clustering was conducted until clusters were at least 2 Å RMSD different from each other. The centroid of each cluster was then used to initialize BPMD simulations.

System preparation for binding pose metadynamics (BPMD). Each selected pose was prepared using CHARMM-GUI.[33] The protein and lipids were represented by the CHARMM36m[34] and CHARMM36 lipid[35] force fields, respectively. Water was presented by the modified TIP3P model[36,37] and ions were represented by the CHARMM sodium/chloride force field.[38] A pure POPC bilayer comprising of approximately 175 lipids per leaflet was created, then μOR with fentanyl or a nitazene derivative in the selected pose was inserted into the bilayer using the PPM 2.0 webserver.[39] Water molecules were added with a layer thickness of 22.5 Å; sodium and chloride ions were added to neutralize the system (based on the protonation states determined in Ref.[24]) and reach an ionic strength of 150 mM. Following the recommended protocol in CHARMM-GUI,[33] the system was minimized over 5000 steps then heated to 300 K over 125 ps with restraints on protein positions, lipid positions, and lipid dihedrals. These restraints were then gradually reduced in steps over 2.25 ns. OpenMM[40] v8.0 was used for both the recommended protocol and metadynamics simulations. A cutoff of 12 Å was used for nonbonded interactions, while long-range electrostatics were calculated using Particle Mesh Ewald summation with the grid size of 1 Å and real-space cutoff of 10 Å. Pressure of 1 bar was applied using the Monte-Carlo barostat[41] with a coupling frequency of 100 steps, with the x and y dimensions coupled isotropically. Unless otherwise specified, temperature was set to 300 K using the Langevin thermostat[42] with a friction coefficient of 1.

SETTLE[43] was used for water molecules while SHAKE[44] was used for all other atoms.

Settings in binding pose metadynamics (BPMD). For BPMD, we followed the protocol of Ludauskis and Gervasio et al.[12] The metadynamics class in OpenMM was used to perform WT-metadynamics.[13] To allow SETTLE[43] and SHAKE[44] algorithms were used for constraining bonds and angles involving hydrogen atoms in water and protein, respectively. A hydrogen mass repartition scheme[45] was applied to the system to allow a timestep of 4 fs. A flat-bottom restraint with a constraint of zero was applied to fix a periodic boundary issue.[12] Ten 10 ns WT-metadynamics[13] simulations were performed for each pose, where the collective variable (CV) was set to the RMSD of the ligand heavy atom positions with respect to those in the first frame of the simulation. The metadynamics parameters were identical to those by Ludauskis et al.:[12] a bias was deposited every 1 ps with a hill height of 0.3 kcal/mol and a width of 0.02 Å, and the bias factor was set to 4. The bias was applied to a grid spanning 0 to 10 Å, with five points per bias width.

Each pose was evaluated according to the time evolution of the ligand RMSD and the minimum distance between the charged amine nitrogen and the carboxylate oxygen of Asp147$^{3.32}$; these quantities were calculated for each frame of one trajectory followed by averaging over the ten independent trajectories.

Binding pose refinement with conventional MD (cMD)

Conventional MD was used to refine the SP2-binding mode for nitro-containing nitazenes. For each molecule, the system was prepared as for initializing BPMD trials followed by the 100-ns (300-ns for etonitazene) cMD simulation using OpenMM[40] v8.0, with the aforementioned MD settings.

μOR-ligand interaction analysis was performed on the last 50 ns of the 100 ns cMD simulation using MDTraj[46] with a heavy-atom distance cutoff of 4.5 Å for hydrophobic contacts and salt bridges, while water-mediated interactions were analyzed using MDAnalysis.[47] All other analysis, such as RMSD calculations, were performed with CPPTRAJ[32]

Estimating the relative stabilities of the SP1 and SP2-binding modes for etonitazene

To sample transitions from SP1- to SP2-binding modes, we first refined etonitazene in SP1 through cMD according to the protocol detailed above. SP1 was selected as we hypothesized that once the nitro group exits the subpocket and moves into the main pocket, Gln124 will move into SP1 thus opening the pathway to SP2. We conducted five 200 ns WT-metadynamics simulations of μOR:etonitazene complex starting from the cMD refined SP1-binding pose. Two CVs were used to represent the progress towards the SP1- and SP2-binding modes. For the former, we used the distance between the nitro group nitrogen and the Cα center of mass (COM) of residues 122-126 on TM2 and 140-144 on TM3. For the latter, we used the distance between the nitro nitrogen and Cα COM of residues 122-126 on TM2 and 319-323 on TM7. In WT-metadynamics, biasing deposits were added every 50 ps with a hill height of 0.25 kcal/mol and a width of 0.25 Å, and a bias factor of 14. PLUMED 2.7[48] was used to run WT-metadynamics in OpenMM and calculate the approximate free energy landscape along the CVs. Pathways from the SP1- to the SP2-binding modes were produced using the nudged elastic band method through a modified script from the R package metadynminer.[49]

Estimating relative stabilities of SP1, SP2, and SP3 binding modes for etodesnitazene

cMD was also used to refine the SP1, SP2, and SP3 binding modes of etodesnitazene. The protocol of refining these modes was the same as refining the SP2-binding mode of nitro-containing nitazenes, except the simulations

were extended to 200 ns. This was done to first refine the pose with 100 ns, then an additional 100 ns for analysis. Three separate simulations were done for each binding mode, for a total of nine simulations. Measured distances were done using the benzimidazole carbon at the 6-position (which connects to the nitro of nitro-containing nitazenes) and the COM of Cα atoms of either residues 122-126 and 140-144 (SP1), residues 122-126 and 319-323 (SP2), or residues 234-238 and 298-302 (SP3). Distances, RMSDs, and dihedrals were calculated using CPPTRAJ[32] while water-mediated hydrogen bonds were analyzed using MDAnalysis.[47] The contacts shown in Figure 8 were found using the final 50 ns of the SP2 pose trajectory indicated in blue in Figure S7; this was done as other nitazene contacts were found using a single trajectory.

Data Availability. The docked and refined poses of all nitazenes as well as all simulation inputs are freely downloadable from GitHub (`https://github.com/janashen/Nitazenes`).

Acknowledgement Joseph Clayton is supported by the ORISE fellowship, which is a Research Participation Program at the FDA administered through the Oak Ridge Institute for Science and Education (ORISE) under the agreement between the FDA and Department of Energy. J.S. is supported by the National Institutes of Health (R35GM148261 and R01CA256557).

Disclaimer. This article reflects the views of the authors and should not be construed to represent FDA's views or policies. The mention of commercial products, their sources, or their use in connection with material reported herein is not to be construed as either an actual or implied endorsement of such products by the FDA.

Supporting Information Available

Table S1 containes the published X-ray structures and cryo-EM models of μOR in complex with agonist ligands. Table S2–S4 contain the docking scores of fentanyl and nitazenes from the three software programs based on two different templates. Table S5 contains the occupancies of the water-mediated hydrogen bonds between the nitro-containing nitazenes and μOR. Fig. S1 compares the experimentally determined binding poses of BU72, DAMGO, fentanyl, and MP. Fig. S2 and S3 contains the BPMD pose evaluation for the nitro-containing (Fig. S2) and nitro-less (Fig. S3) nitazenes. Fig. S4 details the SP2' pose predicted only by Autodock. Fig. S5 contains the approximate free energy surfaces for the transition between SP1 and SP2-binding modes of etonitazene from WT-metadynamics simulations. Fig. S6 contains the time evoluation of CVs and Gln124$^{2.60}$ χ_2 angle in the WT-metadynamics simulations of μOR:etonitazene complex. Fig. S7 contains the time evolution of pocket distances, Gln124$^{2.60}\chi_2$ angle, and etonitazene RMSD in the etodesnitazene cMD simulations. Fig. S8 contains a visualization of an extended etonitazene cMD simulation and the time evolution of the RMSD with respect to the final frame. Fig. S9 contains the time evolution that suggests the possible interaction between the nitro-containing nitazenes and Tyr75$^{1.39}$.

References

(1) Drug Overdose Death Rates. `https://nida.nih.gov/research-topics/trends-statistics/overdose-death-rates`, Accessed May 20, 2024.

(2) Burns, S. M.; Cunningham, C. W.; Mercer, S. L. DARK Classics in Chemical Neuroscience: Fentanyl. *ACS Chem. Neurosci.* **2018**, *9*, 2428–2437.

(3) Comer, S. D.; Cahill, C. M. Fentanyl: Receptor Pharmacology, Abuse Potential,

and Implications for Treatment. *Neurosci. Biobehav. Rev.* **2019**, *106*, 49–57.

(4) Ujváry, I.; Christie, R.; Evans-Brown, M.; Gallegos, A.; Jorge, R.; de Morais, J.; Sedefov, R. DARK Classics in Chemical Neuroscience: Etonitazene and Related Benzimidazoles. *ACS Chem. Neurosci.* **2021**, *12*, 1072–1092.

(5) DEA Washington, DC Division - Public Information Office, New, Dangerous Synthetic Opioid in D.C., Emerging in Tri-State Area. 2022; `https://www.dea.gov/stories/2022/2022-06/2022-06-01/new-dangerous-synthetic-opioid-dc-emerging-tri-state-area`, Accessed: 2023-12-12.

(6) Lists of: Scheduling Actions, Controlled Substances, Regulated Chemicals. `https://www.deadiversion.usdoj.gov/schedules/orangebook/orangebook.pdf`, Accessed: July 8, 2024.

(7) Vandeputte, M. M.; Van Uytfanghe, K.; Layle, N. K.; St. Germaine, D. M.; Iula, D. M.; Stove, C. P. Synthesis, Chemical Characterization, and μ-Opioid Receptor Activity Assessment of the Emerging Group of "Nitazene" 2-Benzylbenzimidazole Synthetic Opioids. *ACS Chem. Neurosci.* **2021**, *12*, 1241–1251.

(8) Kozell, L. B.; Eshleman, A. J.; Wolfrum, K. M.; Swanson, T. L.; Bloom, S. H.; Benware, S.; Schmachtenberg, J. L.; Schutzer, K. A.; Schutzer, W. E.; Janowsky, A.; Abbas, A. I. Pharmacologic Characterization of Substituted Nitazenes at Mu, Kappa and Delta Opioid Receptors Suggests High Potential for Toxicity. *J. Pharmacol. Exp. Ther.* **2024**, JPET–AR–2023–002052.

(9) Tsai, M.-H. M.; Chen, L.; Baumann, M. H.; Canals, M.; Javitch, J. A.; Lane, J. R.; Shi, L. In Vitro Functional Profiling of Fentanyl and Nitazene Analogs at the μ-Opioid Receptor Reveals High Efficacy for Gi Protein Signaling. *ACS Chem. Neurosci.* **2024**, *15*, 854–867.

(10) Amaducci, A. et al. Naloxone Use in Novel Potent Opioid and Fentanyl Overdoses in Emergency Department Patients. *JAMA Netw Open* **2023**, *6*, e2331264.

(11) Clark, A. J.; Tiwary, P.; Borrelli, K.; Feng, S.; Miller, E. B.; Abel, R.; Friesner, R. A.; Berne, B. J. Prediction of Protein–Ligand Binding Poses via a Combination of Induced Fit Docking and Metadynamics Simulations. *J. Chem. Theory Comput.* **2016**, *12*, 2990–2998.

(12) Lukauskis, D.; Samways, M. L.; Aureli, S.; Cossins, B. P.; Taylor, R. D.; Gervasio, F. L. Open Binding Pose Metadynamics: An Effective Approach for the Ranking of Protein–Ligand Binding Poses. *J. Chem. Inf. Model.* **2022**, *62*, 6209–6216.

(13) Barducci, A.; Bussi, G.; Parrinello, M. Well-Tempered Metadynamics: A Smoothly Converging and Tunable Free-Energy Method. *Phys. Rev. Lett.* **2008**, *100*, 020603.

(14) Huang, W. et al. Structural Insights into μ-Opioid Receptor Activation. *Nature* **2015**, *524*, 315–321.

(15) Qu, Q. et al. Insights into Distinct Signaling Profiles of the µOR Activated by Diverse Agonists. *Nat. Chem. Biol.* **2022**,

(16) Ballesteros, J. A.; Weinstein, H. Integrated Methods for the Construction of Three-Dimensional Models and Computational Probing of Structure-Function Relations in G Protein-Coupled Receptors. *Methods Neurosci.* **1995**, *25*, 366–428.

(17) Munro, T. A. Reanalysis of a μ Opioid Receptor Crystal Structure Reveals a Covalent Adduct with BU72. *BMC Biol.* **2023**, *21*, 213.

(18) Zhuang, Y. et al. Molecular Recognition of Morphine and Fentanyl by the Human

μ-Opioid Receptor. *Cell* **2022**, *185*, 4361–4375.e19.

(19) Eberhardt, J.; Santos-Martins, D.; Tillack, A. F.; Forli, S. AutoDock Vina 1.2.0: New Docking Methods, Expanded Force Field, and Python Bindings. *J. Chem. Inf. Model.* **2021**, *61*, 3891–3898.

(20) Friesner, R. A.; Banks, J. L.; Murphy, R. B.; Halgren, T. A.; Klicic, J. J.; Mainz, D. T.; Repasky, M. P.; Knoll, E. H.; Shelley, M.; Perry, J. K.; Shaw, D. E.; Francis, P.; Shenkin, P. S. Glide: A New Approach for Rapid, Accurate Docking and Scoring. 1. Method and Assessment of Docking Accuracy. *J. Med. Chem.* **2004**, *47*, 1739–1749.

(21) Molecular Operating Environment (MOE), 2022.02, Chemical Computing Group ULC. 910-1010 Sherbrooke St. W., Montreal, QC H3A 2R7, Canada.

(22) Ellis, C. R.; Kruhlak, N. L.; Kim, M. T.; Hawkins, E. G.; Stavitskaya, L. Predicting Opioid Receptor Binding Affinity of Pharmacologically Unclassified Designer Substances Using Molecular Docking. *PLoS One* **2018**, *13*, e0197734.

(23) Lipiński, P. F. J.; Jarończyk, M.; Dobrowolski, J. C.; Sadlej, J. Molecular Dynamics of Fentanyl Bound to μ-Opioid Receptor. *J. Mol. Model.* **2019**, *25*, 144.

(24) Vo, Q. N.; Mahinthichaichan, P.; Shen, J.; Ellis, C. R. How μ-Opioid Receptor Recognizes Fentanyl. *Nat. Commun.* **2021**, *12*, 984.

(25) Mahinthichaichan, P.; Liu, R.; Vo, Q. N.; Ellis, C. R.; Stavitskaya, L.; Shen, J. Structure–Kinetics Relationships of Opioids from Metadynamics and Machine Learning Analysis. *J. Chem. Inf. Model.* **2023**, *63*, 2196–2206.

(26) Jonsson, H.; Mills, G.; Jacobsen, K. W. *Classical and Quantum Dynamics in Condensed Phase Simulations*; WORLD SCIENTIFIC, 1998; pp 385–404.

(27) Mahinthichaichan, P.; Vo, Q. N.; Ellis, C. R.; Shen, J. Kinetics and Mechanism of Fentanyl Dissociation from the μ-Opioid Receptor. *JACS Au* **2021**, *1*, 2208–2215.

(28) Madhavi Sastry, G.; Adzhigirey, M.; Day, T.; Annabhimoju, R.; Sherman, W. Protein and Ligand Preparation: Parameters, Protocols, and Influence on Virtual Screening Enrichments. *J. Comput.-Aided Mol. Des.* **2013**, *27*, 221–234.

(29) Morris, G. M.; Huey, R.; Lindstrom, W.; Sanner, M. F.; Belew, R. K.; Goodsell, D. S.; Olson, A. J. AutoDock4 and AutoDockTools4: Automated Docking with Selective Receptor Flexibility. *J. Comput. Chem.* **2009**, *30*, 2785–2791.

(30) Trott, O.; Olson, A. J. AutoDock Vina: Improving the Speed and Accuracy of Docking with a New Scoring Function, Efficient Optimization, and Multithreading. *J. Comput. Chem.* **2009**, 455–461.

(31) Huang, R.; Xia, M.; Cho, M.-H.; Sakamuru, S.; Shinn, P.; Houck, K. A.; Dix, D. J.; Judson, R. S.; Witt, K. L.; Kavlock, R. J.; Tice, R. R.; Austin, C. P. Chemical Genomics Profiling of Environmental Chemical Modulation of Human Nuclear Receptors. *Environ Health Perspect* **2011**, *119*, 1142–1148.

(32) Roe, D. R.; Cheatham, T. E. PTRAJ and CPPTRAJ: Software for Processing and Analysis of Molecular Dynamics Trajectory Data. *J. Chem. Theory Comput.* **2013**, *9*, 3084–3095.

(33) Jo, S.; Kim, T.; Iyer, V. G.; Im, W. CHARMM-GUI: A Web-Based Graphical User Interface for CHARMM. *J. Comput. Chem.* **2008**, *29*, 1859–1865.

(34) Huang, J.; Rauscher, S.; Nawrocki, G.; Ran, T.; Feig, M.; de Groot, B. L.; Grubmüller, H.; MacKerell, A. D. CHARMM36m: An Improved Force Field for Folded and Intrinsically Disordered Proteins. *Nat. Methods* **2017**, *14*, 71–73.

(35) Klauda, J. B.; Venable, R. M.; Freites, J. A.; O'Connor, J. W.; Tobias, D. J.; Mondragon-Ramirez, C.; Vorobyov, I.; MacKerell, A. D.; Pastor, R. W. Update of the CHARMM All-Atom Additive Force Field for Lipids: Validation on Six Lipid Types. *J. Phys. Chem. B* **2010**, *114*, 7830–7843.

(36) Jorgensen, W. L.; Chandrasekhar, J.; Madura, J. D. Comparison of Simple Potential Functions for Simulating Liquid Water. *J. Chem. Phys.* **1983**, *79*, 926–935.

(37) MacKerell Jr., A. D. et al. All-Atom Empirical Potential for Molecular Modeling and Dynamics Studies of Proteins. *J. Phys. Chem. B* **1998**, *102*, 3586–3616.

(38) Beglov, D.; Roux, B. Finite Representation of an Infinite Bulk System: Solvent Boundary Potential for Computer Simulations. *J. Chem. Phys.* **1994**, *100*, 9050–9063.

(39) Lomize, M. A.; Pogozheva, I. D.; Joo, H.; Mosberg, H. I.; Lomize, A. L. OPM Database and PPM Web Server: Resources for Positioning of Proteins in Membranes. *Nucl. Acids Res.* **2012**, *40*, D370–D376.

(40) Eastman, P.; Swails, J.; Chodera, J. D.; McGibbon, R. T.; Zhao, Y.; Beauchamp, K. A.; Wang, L.-P.; Simmonett, A. C.; Harrigan, M. P.; Stern, C. D.; Wiewiora, R. P.; Brooks, B. R.; Pande, V. S. OpenMM 7: Rapid Development of High Performance Algorithms for Molecular Dynamics. *PLOS Comput. Biol.* **2017**, *13*, e1005659.

(41) Åqvist, J.; Wennerström, P.; Nervall, M.; Bjelic, S.; Brandsdal, B. O. Molecular dynamics simulations of water and biomolecules with a Monte Carlo constant pressure algorithm. *Chem. Phys. Lett.* **2004**, *384*, 288–294.

(42) Loncharich, R. J.; Brooks, B. R.; Pastor, R. W. Langevin dynamics of peptides: The frictional dependence of isomerization rates of N -acetylalanyl-N'-methylamide. *Biopolymers* **1992**, *32*, 523–535.

(43) Miyamoto, S.; Kollman, P. A. Settle: An Analytical Version of the SHAKE and RATTLE Algorithm for Rigid Water Models. *J. Comput. Chem.* **1992**, *13*, 952–962.

(44) Ryckaert, J.-P.; Ciccotti, G.; Berendsen, H. J. Numerical integration of the cartesian equations of motion of a system with constraints: molecular dynamics of n-alkanes. *J. Comput. Phys.* **1977**, *23*, 327–341.

(45) Hopkins, C. W.; Le Grand, S.; Walker, R. C.; Roitberg, A. E. Long-Time-Step Molecular Dynamics through Hydrogen Mass Repartitioning. *J. Chem. Theory Comput.* **2015**, *11*, 1864–1874.

(46) McGibbon, R. T.; Beauchamp, K. A.; Harrigan, M. P.; Klein, C.; Swails, J. M.; Hernández, C. X.; Schwantes, C. R.; Wang, L.-P.; Lane, T. J.; Pande, V. S. MDTraj: A Modern Open Library for the Analysis of Molecular Dynamics Trajectories. *Biophys. J.* **2015**, *109*, 1528–1532.

(47) Michaud-Agrawal, N.; Denning, E. J.; Woolf, T. B.; Beckstein, O. MDAnalysis: A Toolkit for the Analysis of Molecular Dynamics Simulations. *J. Comput. Chem.* **2011**, *32*, 2319–2327.

(48) Tribello, G. A.; Bonomi, M.; Branduardi, D.; Camilloni, C.; Bussi, G. PLUMED 2: New Feathers for an Old Bird. *Comput. Phys. Commun.* **2014**, *185*, 604–613.

(49) Trapl, D.; Spiwok, V. Analysis of the Results of Metadynamics Simulations by Metadynminer and Metadynminer3d. *R J.* **2022**, *14*, 46–58.

TOC Graphic

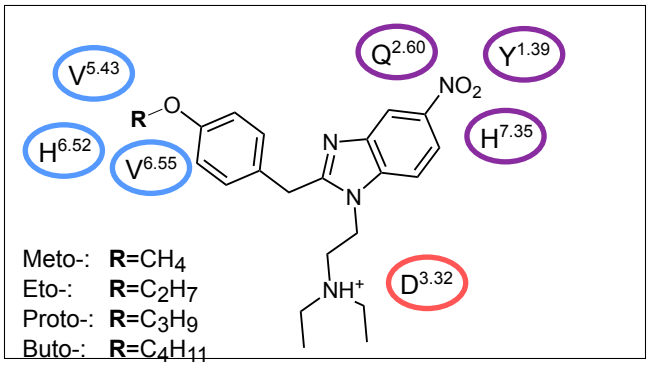
V5.43
Q2.60
Y1.39
NO2
R
O
H6.52
V6.55
N
H7.35
N
Meto-: R=CH4
Eto-: R=C2H7
Proto-: R=C3H9
Buto-: R=C4H11
NH+
D3.32